Journal Pre-proofs

Joule heating of CuO-ZnO/Ni foam catalyst for high H_2 production and energy-saving of methanol decomposition: From the performance to mechanism

Xuechen Zhou, Limo He, Chiyu Wang, Yufan Yang, Yanglin Chen, Song Hu, Sam Fong Yau Li, Yifei Sun, Sheng Su, Yi Wang, Jun Xiang

PII: S1385-8947(25)03151-1
DOI: https://doi.org/10.1016/j.cej.2025.162325
Reference: CEJ 162325

To appear in: *Chemical Engineering Journal*

Received Date: 3 January 2025
Revised Date: 2 April 2025
Accepted Date: 3 April 2025

Please cite this article as: X. Zhou, L. He, C. Wang, Y. Yang, Y. Chen, S. Hu, S.F. Yau Li, Y. Sun, S. Su, Y. Wang, J. Xiang, Joule heating of CuO-ZnO/Ni foam catalyst for high H_2 production and energy-saving of methanol decomposition: From the performance to mechanism, *Chemical Engineering Journal* (2025), doi: https://doi.org/10.1016/j.cej.2025.162325

Joule heating of CuO-ZnO/Ni foam catalyst for high H_2 production and energy-saving of methanol decomposition: From the performance to mechanism

Xuechen Zhou[1], Limo He[1, 2*], Chiyu Wang[1], Yufan Yang[3], Yanglin Chen[4], Song Hu[1, 3], Sam Fong Yau Li[2], Yifei Sun[5], Sheng Su[1, 3], Yi Wang[1, 3], Jun Xiang[1, 3]

1. State Key Laboratory of Coal Combustion, School of Energy and Power Engineering, Huazhong University of Science and Technology, Wuhan 430074, China

2. Department of Chemistry, Faculty of Science, National University of Singapore, 117543, Singapore

3. China-EU Institute for Clean and Renewable Energy, Huazhong University of Science and Technology, Wuhan 430074, China

4. School of Materials Science and Engineering, Nanyang Technological University, 639798, Singapore

5. State Key Laboratory of Physical Chemistry of Solid Surfaces College of Chemistry and Chemical Engineering Xiamen University, Xiamen 361005, China

*Corresponding author. Fax: +86 27 87545526; Tel: +86 27 87542417

E-mail addresses: limo_615@163.com (L. He)

Abstract

Methanol, as a H_2 storage carrier, is a good option to tackle with the challenges of H_2 storage and transportation. To improve hydrogen production and reduce energy consumption, a new approach of electrified methanol decomposition (MD) by Joule heating was investigated in this work. The conductive metal skeleton catalysts were prepared using nickel foam (NF) as a catalyst support and employing a hydrothermal-impregnation method to load the Cu/Zn active components. The catalyst heats up rapidly upon energizing, and the heating rates reaches over 10°C/s. The Joule heating method significantly promotes the methanol conversions of CuO-ZnO/NF, CuO/NF, and ZnO/NF. Methanol conversion over CuO-ZnO/NF at 300°C under Joule heating is over 80% higher than that of conventional external heating, while its energy consumption is only 29% of that under external heating. As a result, methanol conversion per unit power in Joule heating condition increases by 5.6 times compared with that in external heating. The in/ex-situ characterizations reveal that the Joule heating of metal skeleton catalyst promotes the lattice oxygen release of NF skeleton and redox of Cu/Zn species, which generates an extra electrochemical effect on the reaction. This study of Joule heating provides a new strategy of converting methanol to H_2 in a more efficient, energy-saving, and flexible way, and has important application potential in hydrogen energy and chemical energy storage ("Power-to-X").

Keywords:

Joule heating; Methanol decomposition; Hydrogen production; Metal skeleton catalyst; Promoting mechanism

1 Introduction

Currently, the large emission of greenhouse gases (main in the form of CO_2) from the combustion of fossil fuels is exacerbating serious global warming and energy crisis [1, 2]. Hydrogen, as a zero-carbon and clean energy source, will play an important role in powering carbon neutrality and tackling the environmental crisis [3]. However, its low volumetric energy density and high diffusivity [4], pose major challenges in hydrogen storage and transportation, greatly limiting the application of hydrogen energy. Hydrogen storage media, such as methanol [5, 6], methane [7, 8], and ammonia [9], combined with on-site catalytic hydrogen production technology, are considered a promising and feasible approach. Among these, methanol is usually selected because of its convenient storage, high H/C ratio, and the absence of C-C bonds [10, 11]. Particularly, the rising production of biological and zero-carbon methanol is beneficial for the preparation of "green hydrogen" [12-14].

Methanol decomposition (MD) is the fundamental reaction for hydrogen production from methanol. In recent years, copper-based catalysts have been widely used due to their low cost, simple preparation, and high catalytic activity [15]. Among these, $Cu/ZnO/Al_2O_3$ is one of the most common catalysts. The produced gases (primarily H_2 and CO) can be directly burned in the internal combustion engine and gas turbine for power and electricity [16]. However, several issues require further investigation and improvement. Firstly, the catalytic activity of non-precious metal catalysts, such as copper-based ones, is insufficient at low temperature [17, 18]. Hence, improving the low-temperature activity of non-precious metal catalysts is highly significant, as it can reduce the risk of deactivation and lower catalyst costs. Secondly, MD is a highly endothermic reaction, and the decomposition of 1 mole methanol requires the 90.2kJ energy input. For the thermal catalysis of MD, the indirect heating method using an external heater is commonly used, but it suffers from the high heat transfer resistance and large energy loss [19]. Thus, an energy-saving heating approach is another important consideration, which has been usually ignored in the current researches [20]. Thirdly, powder catalysts which are commonly used in current studies cause the high flow resistance and inadequate heat and mass transfer in the catalyst bed [21, 22], leading to reduce catalytic activity and catalyst deactivation due to the carbon deposition [23].

In this work, a novel approach for electrified methanol decomposition using Joule heating is proposed. The conductive catalyst is heated in-situ when an electric current is applied, following the Joule's law. The catalyst, acting as a heater, directly heats the active sites and reactants, and plays the role of activating the reaction as well. This method reduces heat transfer resistance and energy loss compared to the external heating method [24]. Besides, the electrified catalyst may generate additional effect to improve its catalytic activity [25]. In our previous work [26], this method was used to activate the catalyst for volatile organic compounds (VOCs) removal. It was found that

Joule heating improved VOCs conversion compared to external heating at the same reaction temperature. In recent years, the Joule heating method is becoming a research hotspot due to its multiple advantages of high catalytic activity, low energy loss, flexible temperature control, and potential in chemical energy storage, such as in "Power-to-X" applications [27, 28]. It has been used in methane steam reforming (MSR) [29-31], VOCs purification [32-34], ammonia decomposition [35] and CO_2 hydrogenation [36].

The proposed method of electrified methanol decomposition by Joule heating has good potential to improve catalytic activity and reduce energy consumption. But until now, no studies have been reported on Joule heating catalytic MD. Particularly, the promoting mechanism of Joule heating is still unclear. The bifunctional material serving as both catalyst and heater in this process require further investigation. Thus, in this work, a 3D porous metal skeleton catalyst was developed using nickel foam (NF) as the catalyst support, with Cu/Zn loaded via a hydrothermal-impregnation method. The conductive metal skeleton catalyst produces in-situ Joule heating, and its regular 3D network structure and high porosity would reduce flow resistance and enhance mass transfer [37, 38]. Besides, various catalysts, including CuO-ZnO/NF, CuO/NF, and ZnO/NF, were compared under both Joule heating model and conventional external heating model. The catalytic activity and energy consumption performances under Joule heating and external heating were evaluated. Various ex-situ characterizations, in-situ X-ray photoelectron spectrometer (XPS), and in-situ Raman spectroscopy were applied to elucidate the promoting mechanism of Joule heating.

2 Materials and methods

2.1 Catalyst preparation

The nickel foam (NF, thickness 1.6mm, porosity PPI 110) is from Lizhiyuan Battery Material Co., LTD in Shanxi, China. It was cut into strip-shaped pieces of 50 mm×20 mm. They were soaked in the 1mol/L HCl solution for 20 min, then treated by ultrasonic cleaning for 20 min with deionized water and anhydrous ethanol, respectively. These steps were used to remove surface oxides and residual organic impurities. The samples were dried in an oven at 80°C for 3 h, resulting in the preparation of pre-treated NF pieces.

The CuO-ZnO/NF catalysts were prepared via a hydrothermal-impregnation method (Fig. S1). Firstly, the pre-treated NF was added to a 0.03 mol/L $ZnCl_2$ solution and transferred to a 150 mL polytetrafluoroethylene-lined autoclave. The autoclave was sealed and heated at 180°C for 3 h. After cooling to room temperature, the sample was rinsed at least three times with deionized water and dried in a vacuum oven at 80°C for 3 h. The resulting catalyst precursor was designated as Zn/NF-fresh. Then, the Zn/NF-fresh was impregnated in a 0.1 mol/L $CuCl_2 \cdot 2H_2O$ solution at room temperature for 3 h. The sample was rinsed several times with deionized water and dried at 80°C for 3 h.

The obtained catalyst precursor was labelled as CuZn/NF-fresh. For comparison, the pre-treated NF was directly impregnated in a 0.1 mol/L $CuCl_2 \cdot 2H_2O$ solution to prepare the Cu/NF-fresh catalyst precursor. The three precursors of CuZn/NF-fresh, Zn/NF-fresh, and Cu/NF-fresh were calcined in a muffle furnace at 400°C for 1 h at a heating rate of 10°C/min, followed by natural cooling to room temperature. The final catalysts obtained were CuO-ZnO/NF, ZnO/NF, and CuO/NF, respectively (Fig. S2). All chemical reagents used were of analytical grade and purchased from Aladdin Chemical Co., Ltd. (Shanghai).

2.2 Catalytic performance evaluation

The catalytic performance evaluation system for MD is shown in Fig. 1a. During the experiment, methanol was firstly injected into the vaporization chamber by a micro-injection pump at a flow rate of 0.02 mL/min. The gas-phase methanol was carried by the N_2 (purity 99.99%) gas with a flow rate of 50 mL/min, and flowed into the reactor. After the reaction, the unreacted methanol and condensable products were removed by the ice-salt baths and anhydrous ethanol. The produced gases were collected in a gas sampling bag and then analyzed by a gas chromatograph equipped with a thermal conductivity detector (TCD) and a flame ionization detector (FID).

The reactor was self-designed for the Joule heating model and external heating model, as shown in Fig. 1b and c. A prepared catalyst (about 0.4 g) is fixed at the center of a quartz tube reactor by using two copper electrodes which are positioned on either side and connected to a DC power supply. In the Joule heating model (denoted as JH, Fig. 1b), the metal skeleton catalyst generated Joule heating, with its temperature controlled by adjusting the applied voltage within a range of 0 to 3 V. The power supply was operated in constant voltage input mode. A K-type thermocouple was inserted into the catalyst layer to measure the catalyst temperature in real time. In the external heating model (denoted as EH, Fig. 1c), the catalyst was heated by an external fiberglass heating band wrapped around the quartz tube, with no electric current applied to the catalyst. Besides, the thermal insulation tape was wrapped outside the tube to reduce the heat loss, which is not illustrated in the figure. All the tests were conducted at least three times to ensure the accuracy.

After the experiments, methanol conversion rate (X_{MeOH}), H_2 yield (Y_{H_2}) and gas selectivity (S_{H_2} and S_{CO}) are calculated by using the following equations:

$$X_{MeOH}(\%) = \frac{F_D \times (y_{CO} + y_{CO_2}) \times 32}{F \times \rho \times 22.4 \times 1000} \times$$

$$Y_{H_2}(mL \cdot g^{-1} \cdot min^{-1}) = \frac{F_D \times y_{H_2}}{\mathbb{m}_{cat}}$$

154 $$S_{H_2}(\%) = \frac{y_{H_2}}{y_{H_2} + 2 \times y_{CH_4}} \times$$

155 $$S_{CO}(\%) = \frac{y_{CO}}{y_{CO} + y_{CO_2} + y_{CH_4}} \times$$

156 where, $F_D\ (mL/min)$ is the flow rate of decomposition gas, $F\ (mL/min)$ is the feed
157 flow rate of methanol, $\rho\ (g/cm^3)$ is the density of methanol, $\mathbb{m}_{cat}\ (g)$ is the mass of
158 catalyst, and $y_i\ (\%)$ is the volume fraction of decomposition gas.

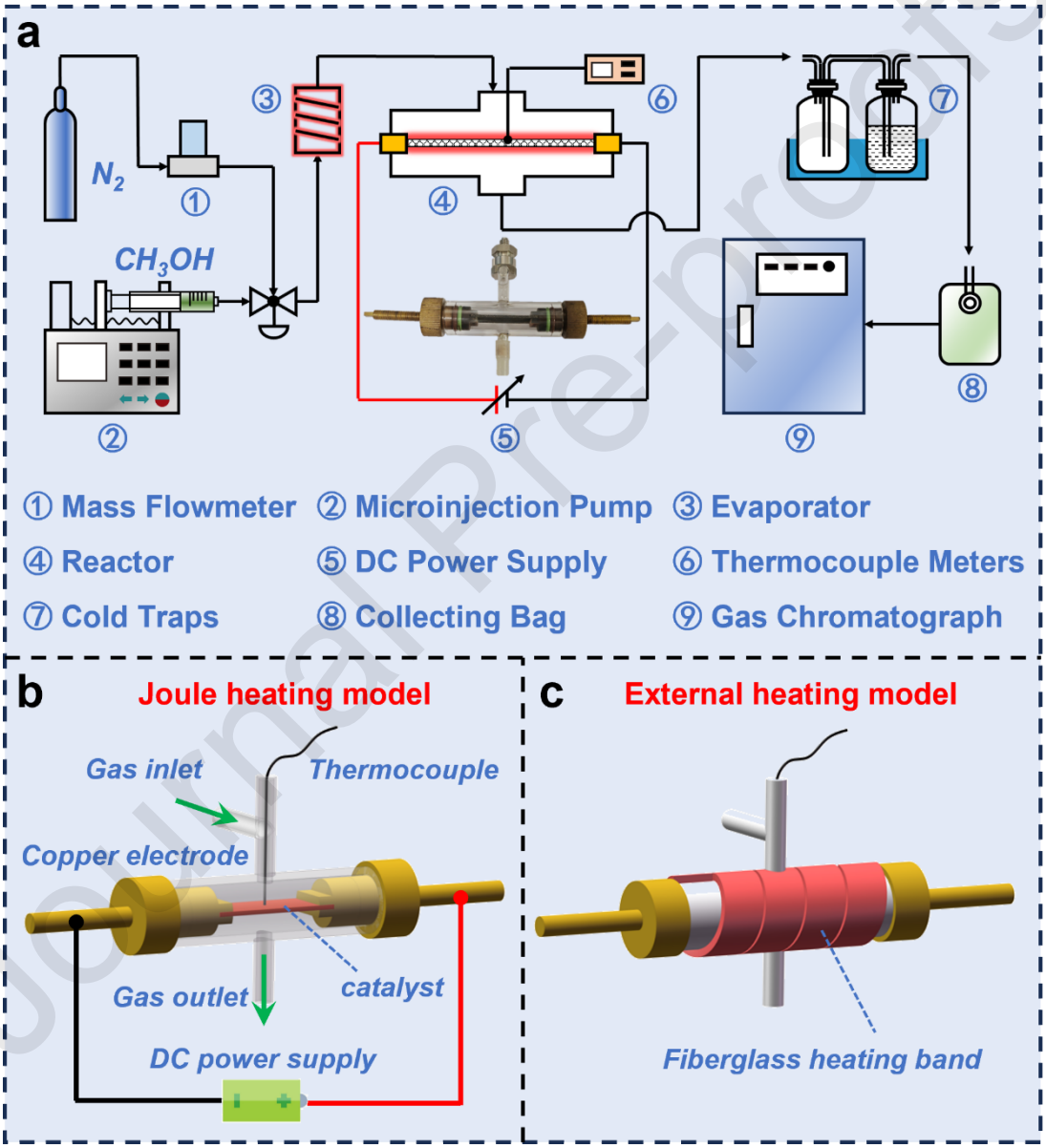

159

160 **Fig. 1.** (a) Catalyst performance evaluation system. Schematic diagram of (b) Joule
161 heating model and (c) external heating model.

2.3 Catalyst characterizations

Grazing Incidence X-ray diffraction (GIXRD) patterns were performed on a SmartLab 9 kW X-ray diffractometer, using Cu Kα radiation (λ=1.5418 Å), with an incident angle of 0.5°, a step size of 0.01°, and a scanning speed of 5° per minute. Raman spectra were obtained on a Fisher DXR2 spectrometer by employing a 532 nm excitation source with a laser power of 2 mW. Scanning electron microscopy (SEM) images were recorded on a Sigma 300 scanning electron microscope operated at 2 kV, and equipped with an Aztec X-Max 80 energy-dispersive X-ray spectrometer (EDS) detector. Transmission electron microscopy (TEM) measurements were performed using a JEM-F200 field emission transmission electron microscope. X-ray photoelectron spectroscopy (XPS) measurements were obtained on an AXIS SUPRA+ system with an Al Kα X-ray line (hν =1486.6 eV). The binding energy of the C 1s peak at 284.8 eV was considered as an internal reference. Inductively coupled plasma mass spectrometry (ICP-MS) measurements were performed using an iCAP TQ mass spectrometer to determine the actual Cu and Zn loading amounts of catalysts. O_2 temperature programmed desorption (O_2-TPD) was performed using a ChemiSorb 2720 chemical adsorption analyzer from Micromeritics. The loading strength of catalyst was tested using a YM-100PLUS ultrasonic cleaner.

In-situ XPS experiments were performed using a SPECS NAP-XPS near-ambient-pressure X-ray photoelectron spectrometer from Germany, with an Al Kα radiation source. Due to the power supply mode of the in-situ cell, the test could not provide the current that met the actual experimental requirements. To ensure the safety of the instrument, a current of 10 mA was used along with laser heating to maintain the catalyst temperature stable at 300°C. The XPS spectra of the catalyst before, during, and after the power supply were recorded. The obtained data were calibrated against the Au $4f_{7/2}$ peak at 84.0 eV.

In-situ Raman experiments were carried out in a custom-made polyether ether ketone (PEEK) reaction chamber. A catalyst with a diameter of 30 mm was tightly pressed against the brass electrode using a quartz block. The reaction chamber was then sealed, and N_2 (purity 99.99%) was passed through the catalyst in a top-to-bottom direction. Before the test, N_2 was purged at room temperature for 10 min to remove impurities, and the spectrum of the original sample was recorded. Then, the current was incrementally adjusted every 20 min to obtain Raman spectra at 5 A, 10 A and 15 A. During the test, a 5×5 μm^2 plane was selected for scanning with a step size of 5 μm. The Raman spectra from the 4 obtained points were averaged to determine the overall chemical structural characteristics of the catalyst.

3 Results and discussion

3.1 Catalyst structures

Crystal structures of ZnO/NF, CuO/NF and CuO-ZnO/NF catalysts are shown in Fig. 2a. The peaks of metal Ni in NF substrate at 44.6°, 51.9° and 76.6° are clearly observed [39]. Low intensity peaks of NiO are also detected owing to the oxidization of surface metal Ni during calcination. For ZnO/NF and CuO-ZnO/NF catalysts, the characteristic peaks of ZnO (JPCDS 70-2551) are observed at 31.9°, 34.5°, and 36.3°, corresponding to the (100), (002), and (101) crystal planes, respectively. Similarly, CuO (JPCDS 45-0937) peaks are observed at 32.5°, 35.6°, and 38.7° for CuO/NF and CuO-ZnO/NF, corresponding to the (110), (002), and (111) crystal planes. The CuO-ZnO/NF catalyst, prepared via a two-step method, exhibits reduced ZnO peak intensity due to the coverage of surface Zn by Cu loading.

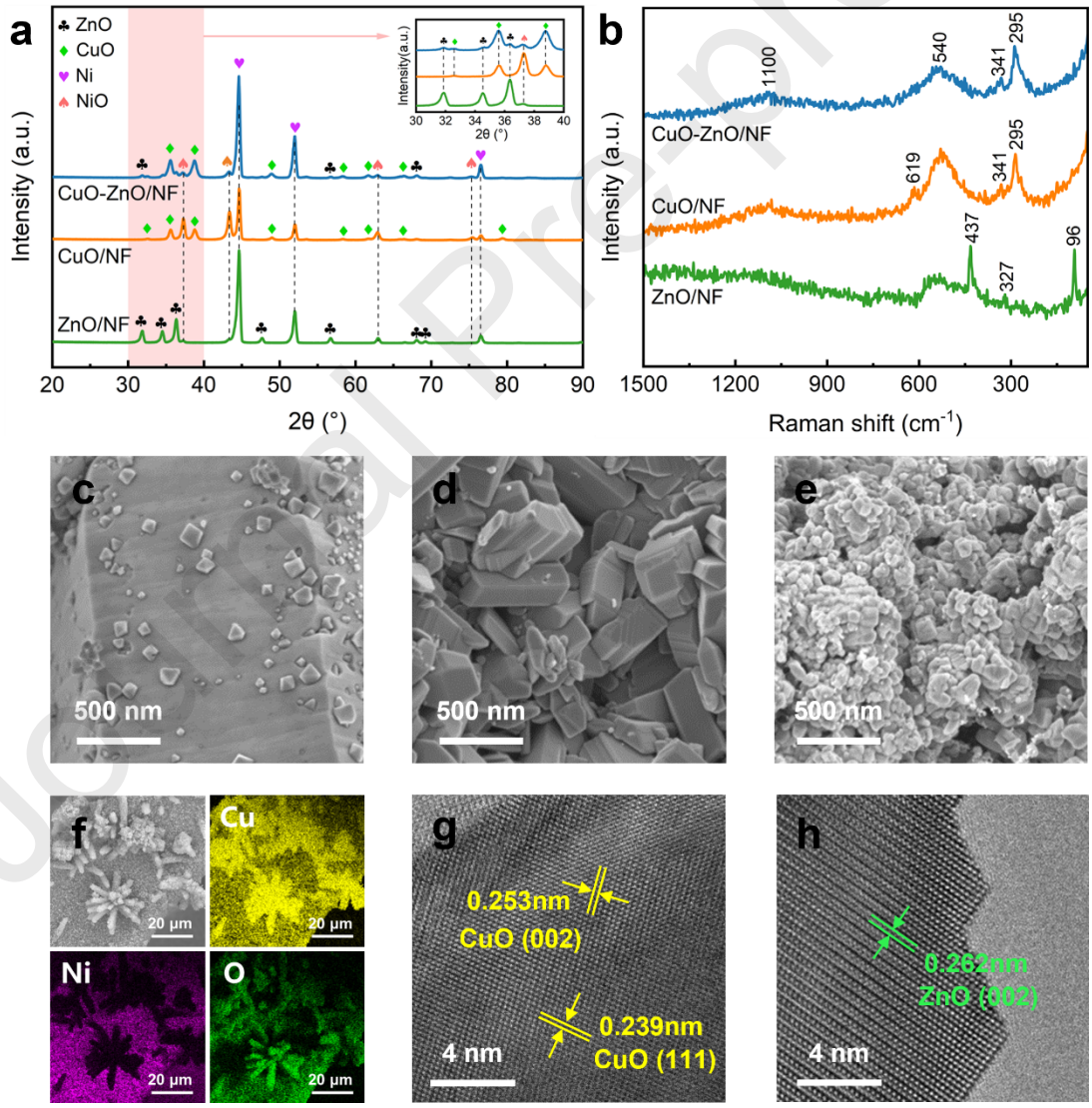

Fig.2. (a) XRD patterns of fresh catalysts. (b) Raman spectra of fresh catalysts. High-

magnification SEM images (×40000): (c) ZnO/NF, (d) CuO/NF and (e) CuO-ZnO/NF. (f) EDS mappings of CuO-ZnO/NF catalyst. TEM images of CuO-ZnO/NF catalyst: (g) CuO crystal face and (h) ZnO crystal face.

The catalyst structure was further characterized by Raman spectroscopy. As shown in Fig. 2b, the 540 cm^{-1} peak in all the catalysts corresponds to the longitudinal optical phonon (LO) mode of NiO, attributed to defect structures [40]. The brod peak at 1100 cm^{-1} is related to the lattice vibration of NiO [41]. In ZnO/NF catalyst, the peaks at 96 cm^{-1} (E_2(low)) and 437 cm^{-1} (E_2(high)) correspond to the lattice vibrations of Zn and O in ZnO [42]. For CuO-ZnO/NF and CuO/NF catalysts, peaks at 295 cm^{-1} and 341 cm^{-1} are assigned to the A_{1g} and B_{1g} modes of CuO, respectively [43]. The peak at 619 cm^{-1} (B_{2g}) on CuO/NF catalyst corresponds to the stretching vibration of Cu-O [44]. Notably, the E_2(high) peak of ZnO is also detected on CuO-ZnO/NF (Fig. S3), confirming the coexistence of CuO and ZnO on the CuO-ZnO/NF catalyst surface. Moreover, the Raman spectrum of CuO on CuO-ZnO/NF shows a redshift, possibly due to the smaller Cu grain size compared with that on CuO/NF [45].

SEM images of ZnO/NF, CuO/NF, and CuO-ZnO/NF catalysts are shown in Fig. 2c-e and Fig. S4. The 3D porous structure of NF substrate is clearly observed in all three catalysts (Fig. S4). A smooth, rod-like array is observed on the ZnO/NF catalyst surface, confirmed as ZnO by EDS analysis (Fig. S5a). The ZnO rods have diameters of 1~4 μm and lengths of about 10 μm. Differently, the CuO/NF catalyst exhibits numerous CuO particles with edge lengths of 200~500 nm. However, the NF substrate is etched after Cu loading (Fig. S4d and e), reducing its mechanical strength. The CuO-ZnO/NF (Fig. 2e) catalyst prepared via a two-step method exhibits a unique morphology of rod-like ZnO coated with CuO nanoparticles. The CuO particle size (70~100 nm) is much smaller than that on CuO/NF, suggesting that Zn promotes CuO dispersion. EDS mapping in Fig. 2f further confirms that CuO predominantly covers the rod-like ZnO surface. TEM images of CuO-ZnO/NF are shown in Fig. 2g and h. The parallel fringes with d-spacings of 0.253 nm and 0.239 nm corresponding to the (002) and (111) planes of monoclinic CuO respectively are detected [46]. Meanwhile, it observes the (002) plane of wurtzite-structured ZnO [47].

The element amounts of Cu and Zn determined by ICP-MS are listed in Table S1. The results show that the Zn and Cu loading amounts in ZnO/NF and CuO/NF are 5.36 wt% and 16.99 wt%, respectively. While in CuO-ZnO/NF, the loading amounts of Zn and Cu are 4.15 wt% and 8.47 wt%. Notably, the total and surface amounts of Zn and Cu in CuO-ZnO/NF are lower than those in the single-metal catalysts, with Cu content consistently higher than Zn. In the load strength test, the ZnO/NF, CuO/NF, and CuO-ZnO/NF catalysts in Fig. S6 exhibited mass losses of 0.9%, 15.4%, and 3.3%, respectively, after 10 min of ultrasound. The results show that the ZnO/NF catalyst,

prepared by the hydrothermal method, demonstrates stronger bonding between the metal coating and the support. In contrast, the impregnation method results in weaker adhesion of the active metal due to the partial stripping of the NF skeleton.

3.2 Joule heating performance of catalyst

The Ni foam and prepared catalysts exhibit good electrical conductivity. Their resistances at different temperatures are shown in Fig. 3a. They were calculated based on the Ohm's law and the voltage-current curves are shown in Fig. S7. The resistances of catalysts consisting of NF covered by active metals are higher than that of the NF substrate. It indicates that the current can flow through both the NF substrate skeleton and the supported catalyst layer. Besides, the different supported metals influence the resistance. The resistance of ZnO/NF is the highest, while CuO-ZnO/NF has higher resistance than CuO/NF. With the rising of temperature from 200°C to 400°C, the resistance of NF is stable, while those of the three catalysts are obviously increased from 0.08 to 0.11 Ω, as shown in Fig. 3a. The catalysts with the loading of Cu and Zn become more sensitive to temperature.

Then, the Joule heating performances of these conductive catalysts are analyzed. Fig. 3b illustrates the surface temperature distribution of the CuO-ZnO/NF catalyst during in-situ Joule heating, which are captured by an infrared thermography. Owing to the excellent thermal conductivity of NF, the region between the two electrodes exhibits a uniform temperature distribution without any obvious transverse temperature gradient. The catalyst is heated to 210°C when applying 15 A current and 1.40 V voltage, whereas it reaches about 380°C with 18 A and 1.90 V.

The temperature curves of the heating processes at 15~18 A and the corresponding cooling processes are shown in Fig. 3c. The temperature curves show the trend of sharply increasing and then slowly turning stable. The catalyst exhibits excellent Joule heating property. The temperature of CuO-ZnO/NF catalyst increases rapidly from 40°C to 300°C within 40 s when an 18 A current is applied. The heating and cooling rates for the Joule heating model are calculated, and shown in Fig. 3d. It can be seen that the maximum heating rate reaches about 12°C/s, and the corresponding maximum cooling rate is about 17°C/s.

For comparison, the external heating method of CuO-ZnO/NF catalyst has been tested, as shown in Fig. 3e. Its maximum heating rate is only 1.2°C/s which is remarkably lower than that of Joule heating (12°C/s). The conventional external heating method takes 10 times longer to reach the same catalyst temperature as Joule heating. Similarly, its cooling rate is much slower, likely due to high heat transfer resistance between the external heater and catalyst. As a result, the external heating model just completes 1 start-stop cycle from 40°C to 300°C, while the Joule heating can complete 8 cycles in the same time (Fig. 3e). Joule heating exhibits significantly faster heating and cooling rates compared to external heating, confirming its high efficiency and rapid

response in electricity-to-heat conversion. Besides, Fig. 3f shows the relationships between catalyst temperature and input power for both heating methods. The power-temperature factor (PTF) of Joule heating over CuO-ZnO/NF is 9.5°C·W^{-1}, while that of external heating is only 3.0°C·W^{-1}. This indicates that Joule heating requires significantly less electricity input than external heating to reach a specific catalyst temperature. The Joule heating of catalyst is an energy-saving way, which will be discussed in detail in the next part.

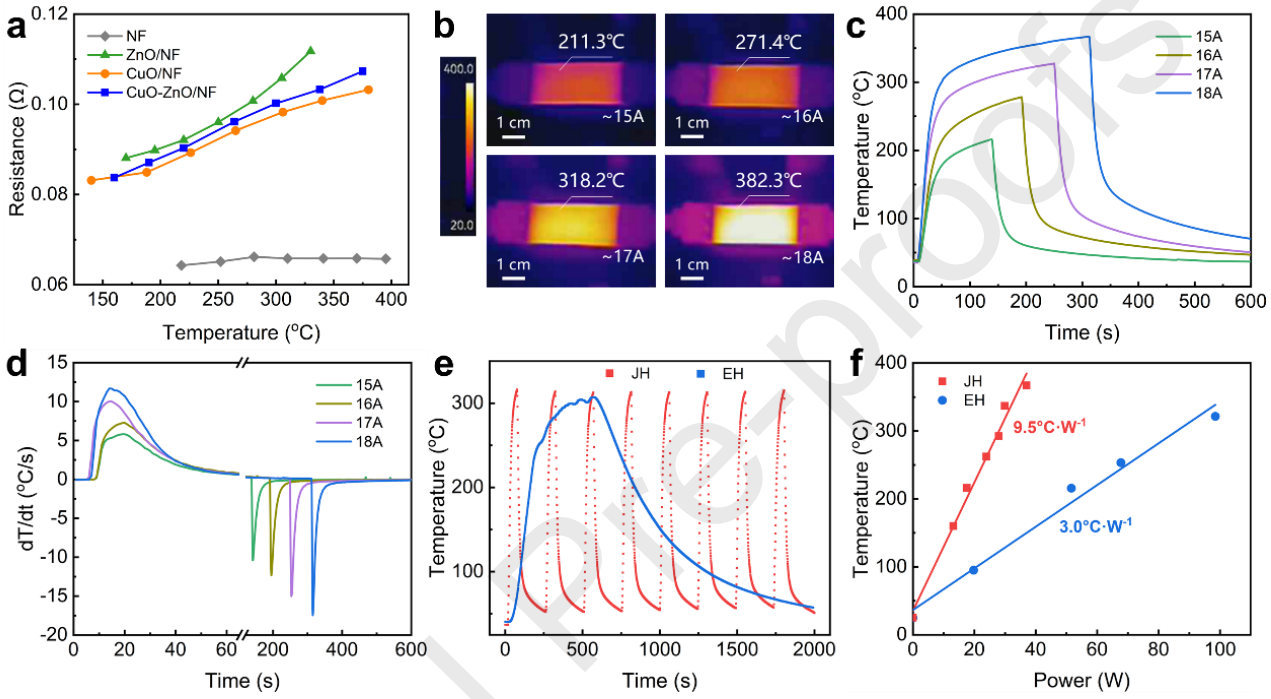

Fig. 3. (a) Resistance-temperature curves of catalysts. (b) Infrared thermograph of the system consisting of a CuO-ZnO/NF catalyst and two electrodes at 15~18 A. (c) The temperature curves of the CuO-ZnO/NF catalyst at 15~18 A input current. (d) Derivative curves of the CuO-ZnO/NF catalyst temperature with respect to time at 15~18 A. (e) Temperature start-stop response curves of the CuO-ZnO/NF catalyst under different heating methods. (f) Temperature response to input power under Joule heating and external heating.

3.3 Catalytic performance and energy consumption

The catalytic performance of MD under Joule heating and external heating was evaluated with the increasing of reaction temperature. The results of CuO-ZnO/NF, ZnO/NF, and CuO/NF catalysts are shown in Fig. 4a-c, respectively. The methanol conversion rate and H_2 yield increase gradually with rising temperature. It is worth noting that catalytic performances of the three catalysts are significantly enhanced under Joule heating compared to external heating. Among them, the CuO-ZnO/NF catalyst under Joule heating exhibits the highest catalytic activity and H_2 yield, with the methanol conversion rate of 82.5% and the H_2 yield of 45.4 ml/g_{cat}/min (Fig. 4d) at 360°C. The gas products primarily consist of H_2, CO, and trace amounts of CO_2 and

CH_4. As shown in Table S2, Joule heating achieves higher selectivity for H_2 and CO, along with a higher H_2/CO ratio, at temperatures below 300°C. This suggests that Joule heating effectively suppresses the formation of gaseous byproducts at low temperatures. Furthermore, the catalytic performance of NF substrate was also evaluated. As shown in Fig. S8, its methanol conversion rate is less than 2% by external heating, and that of Joule heating slightly increases but is still below 5%. This suggests that the metals of Cu and Zn are the main active sites for MD.

Besides, the Joule heating method remarkably enhances the catalytic activity for MD. As shown by the red dotted line in Fig. 4b, the methanol conversion rate over ZnO/NF catalyst under Joule heating at 300°C (16.4%) is about 10 times higher than that under external heating (1.7%). The enhancing effect of Joule heating initially increases with temperature but decreases at higher temperatures, particularly below 300°C. If replacing the external heating by Joule heating, the T_{50} (T_X represents the corresponding catalyst temperature when methanol conversion rate reaches X%) for CuO-ZnO/NF and CuO/NF catalysts is reduced by 41°C and 56°C, respectively. The T_{20} of ZnO/NF catalyst is reduced by 65°C. It indicates that the Joule heating method can improve the low-temperature activity of catalysts, and is helpful to lower the reaction temperature required for MD. Moreover, the promoting effect of Joule heating is more pronounced for ZnO/NF catalyst compared to CuO/NF and CuO-ZnO/NF. There exists a strong interaction between active metals and Joule heating. The type of active component influences the promoting effect of Joule heating.

The apparent activation energy (E_a) for MD in both Joule heating and external heating conditions was calculated, as presented in Fig. 4e and Table S3. The E_a of CuO-ZnO/NF (34.45 kJ/mol) and ZnO/NF (83.89 kJ/mol) under Joule heating is lower than that under external heating (45.28 kJ/mol for CuO-ZnO/NF and 96.77 kJ/mol for ZnO/NF). But the E_a of CuO/NF (58.86 kJ/mol) in Joule heating is higher than that in external heating (48.70 kJ/mol). These results show that CuO-ZnO/NF and CuO/NF has higher catalytic activity than ZnO/NF due to their lower apparent activation energies. Compared with the external heating, Joule heating reduces the Ea for CuO-ZnO/NF and ZnO/NF. Interestingly, the Joule heating increases the E_a of CuO/NF while obviously enhancing its methanol conversion rate. From the Arrhenius equation, it is well known that the E_a value and reaction temperature are two separate factors influencing the reaction rate. The E_a in heterogeneous catalysis is mainly influenced by the catalyst which determines the reaction pathway. Therefore, the changing of E_a is attributed to the evolution of catalyst property under the Joule heating. Besides, the high methanol conversion rate under Joule heating is due to both the lower Ea and the "hotspots" phenomenon, which creates localized high temperatures at the contact surface of catalyst particles [48-50]. These promoting effects of Joule heating will be further discussed in Part 3.4.

The catalytic stability of CuO-ZnO/NF at 300°C was evaluated. As shown in Fig.

4f, the methanol conversion rate under the two heating methods remains stable for 1 h. After 3 h, the conversion rate under Joule heating stays nearly constant, but the external heating rate drops from 36.3% to 29.2%. By 5 h, the conversion rate under Joule heating begins to decline (9.3%), while the external heating rate drops sharply (20.5%). These results clearly show that Joule heating provides better stability than external heating. After 7 h, the conversion rate under Joule heating obviously decreases due to carbon deposition.

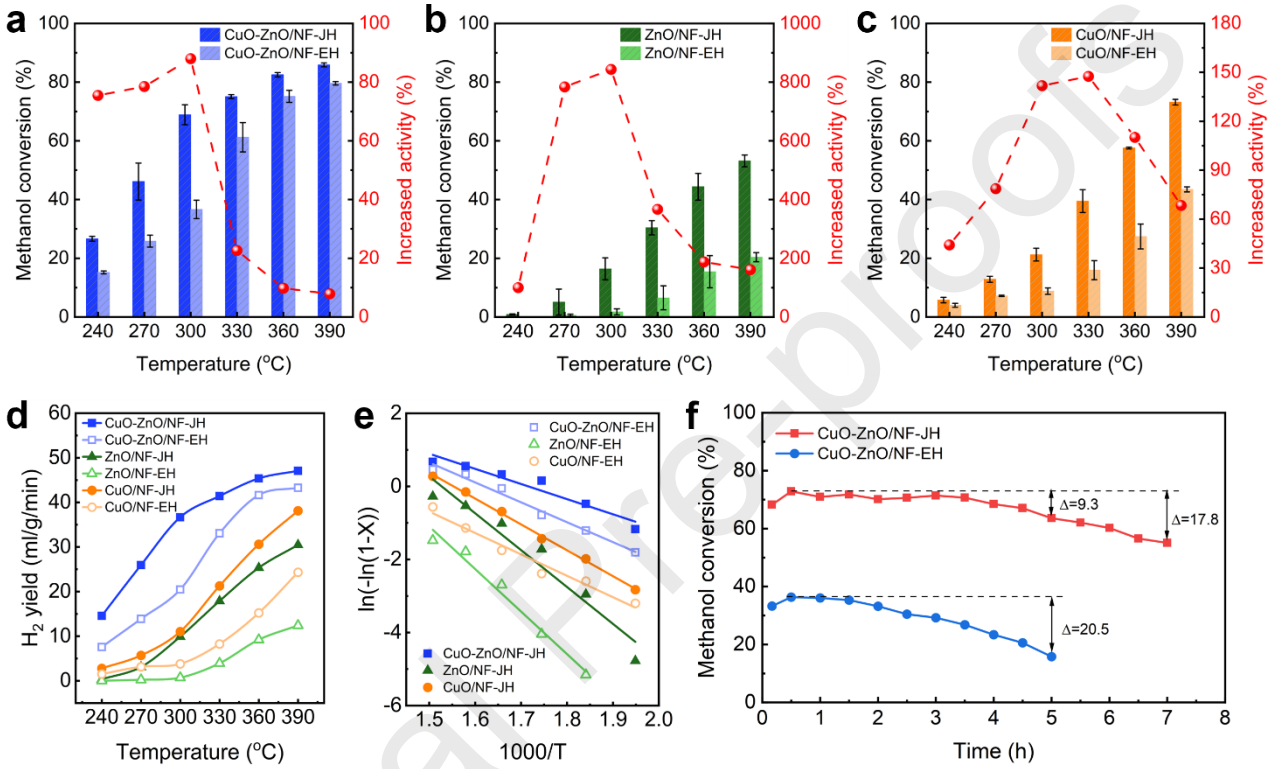

Fig. 4. Comparison of the MD performances under Joule heating and external heating at various temperatures over (a) CuO-ZnO/NF, (b) ZnO/NF and (c) CuO/NF. (d) H_2 yields at different temperatures. (e) Arrhenius plots of three catalysts under Joule heating and external heating. (f) Long time test of CuO-ZnO/NF catalyst under Joule heating and external heating at 300°C.

In addition to Joule heating and external heating, two hybrid heating models combining both were tested. Four heating models of CuO-ZnO/NF catalysts were evaluated by adjusting the proportions of Joule heating and external heating to maintain the catalyst temperature at 300°C. The input energy proportions and test conditions are detailed in Fig. S9 and Table S4. From Model I to Model IV, the proportion of external heating gradually decreases, while the proportion of Joule heating correspondingly increases from 0 to 100%. As shown in Fig. 5a, methanol conversion gradually improves with the increase of voltage. The methanol conversion rate under Joule heating at 300°C is 1.88 times higher than under external heating. The high proportion

of Joule heating not only enhances catalytic activity but also saves energy. Joule heating (Model IV) requires only 27.3 W of total input power, remarkably lower than the 94.6 W needed for external heating (Model I). At 300°C, Joule heating consumes only 29% of the energy used by external heating. Thus, the methanol conversion per unit power sharply increases from Model I to Model IV, with Joule heating achieving 6.6 times higher than external heating.

Fig.5.

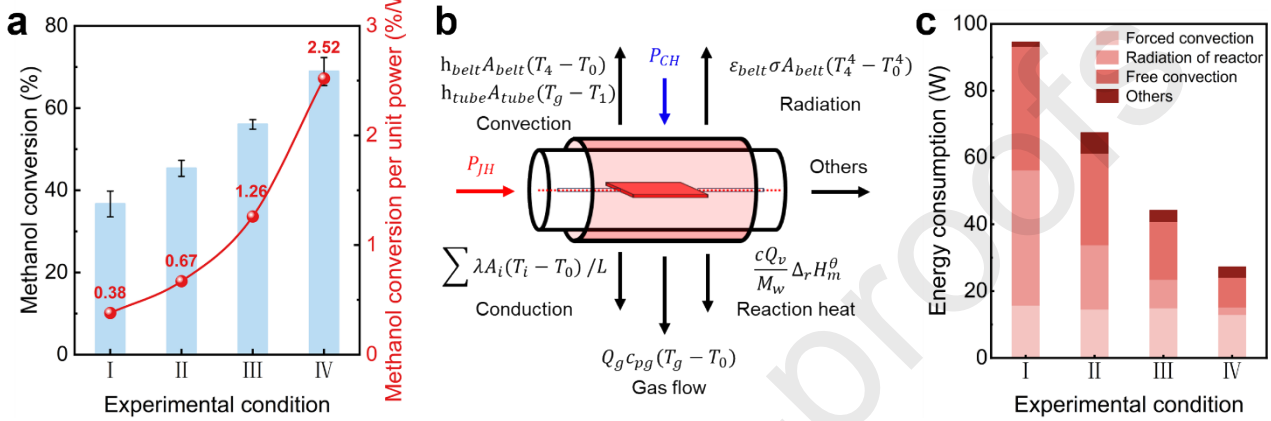

(a) Methanol decomposition performances over CuO-ZnO/NF catalyst under four heating models (T=300°C: I, external heating; II, hybrid heating 1; III, hybrid heating 2; IV, Joule heating). (b) Energy balance diagram. (c) Distribution of Energy loss.

To elucidate the distribution of energy consumption, the heat transfer calculation has been conducted. As shown in Fig. 5b, the total input energy, including Joule heating and external heating, is counterbalanced through various paths: forced convection within the tube, heat transfer between the quartz tube and heating band, free convection external to the tube, tube exterior radiation, heat capacity of gas flow, and reaction heat required for MD [33, 37]. Fig. 5c and Table S5 show the heat losses under the above four heating modes. The Joule heating method significantly reduces heat loss from free convection and radiative heat transfer. As shown in Fig. S10, when maintaining the same catalyst temperature and increasing the Joule heating ratio by 25%, it reduces the surface temperature from 283.7°C (Model I) to 173.2°C (Model II). As the input voltage increases, both the input energy and the reactor surface temperature gradually decrease. When replacing external heating with Joule heating (Model IV), the surface temperature of the reactor reduces by over 200°C. This difference results from the distinct heating mechanisms. In Joule heating model, the catalyst is directly heated by itself when current is applied, and the heat transfers outward from the catalyst to the reactor. In contrast, external heating uses a fiberglass heating belt wrapped around a quartz tube to transfer heat inward. The heater temperature exceeds that of the catalyst due to the heat transfer resistance. The lower surface temperature under Joule heating significantly reduces the energy loss of external free convection and radiative heat transfer. Therefore, Joule heating is an efficient heating method with less energy

consumption.

3.4 Promoting effects of Joule heating

Compared with the external heating, Joule heating remarkably improves the conversion of MD. To clarify the promoting effect of Joule heating, the ex/in-situ XPS and in-situ Raman were conducted. Three catalysts were treated under Joule heating and external heating for 1 h in pure N_2 at 300°C. Their XPS spectra and elemental proportions are shown in Fig. 6 and Table S6. The binding energy of Zn $2p_{3/2}$ is approximately 1021 eV. Given the minimal binding energy difference between Zn^0 and Zn^{2+} in the 2p orbital, the Auger spectrum is utilized to ascertain the chemical state of Zn. As shown in Fig. 6a, the Zn LMM Auger spectrum displays two distinct peaks, assigned to Zn^{2+} at 987.8 eV and Zn^0 at 991.1 eV [46, 51]. The Cu 2p peak pattern in Fig. 6b exhibits a strong satellite peak between 938 eV and 946 eV, which indicates the presence of Cu^{2+} on the catalyst surface [52]. The Cu $2p_{3/2}$ peak near 933.8 eV was deconvoluted, with peaks at 934.4 eV and 933.0 eV attributed to Cu^{2+} and Cu^+/Cu^0, respectively [53]. Combined with the O 1s XPS spectrum in Fig. 6c, the subpeaks at 532.0 eV, 530.9 eV, and 529.3 eV correspond to adsorbed oxygen species (O_{ad}) and lattice oxygen (O_{lat}) in Zn-O and Ni-O, respectively [54, 55].

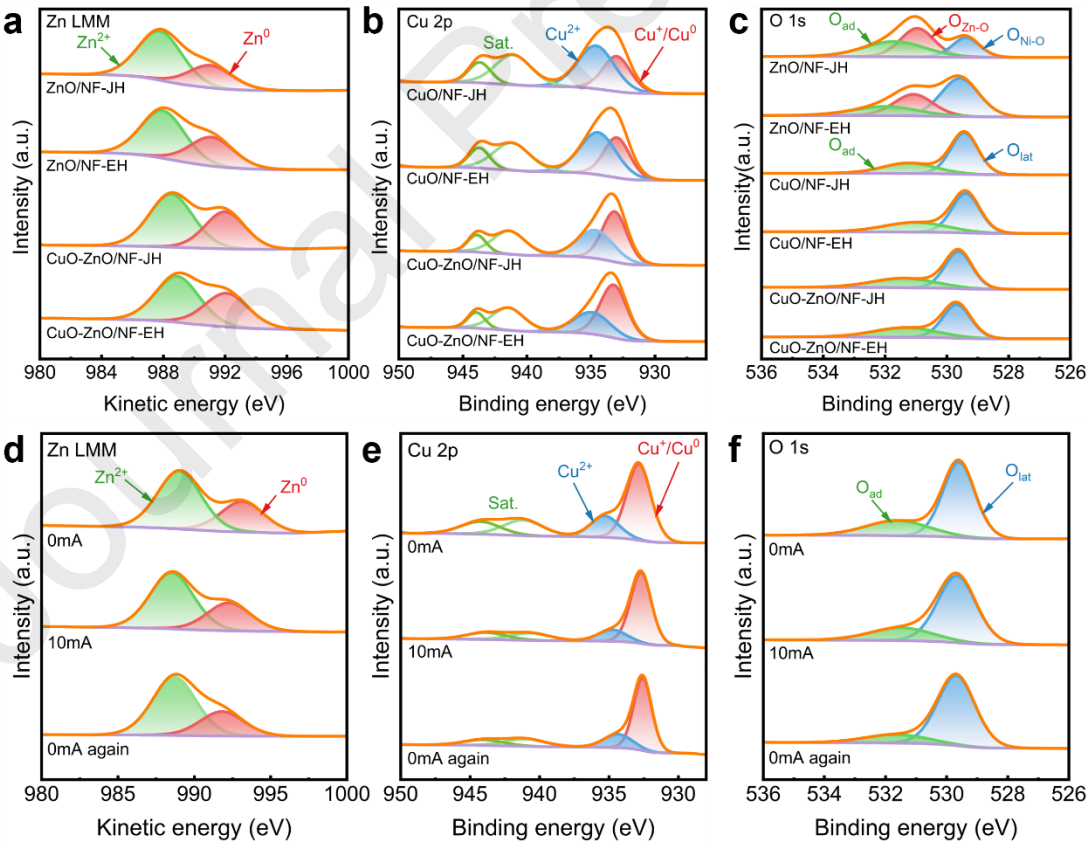

Fig. 6. XPS spectra of three catalysts after Joule heating and external heating: (a) Zn LMM, (b) Cu 2p and (c) O 1s. In-situ XPS spectra of CuO-ZnO/NF catalyst under

electrification: (d) Zn LMM, (e) Cu 2p and (f) O 1s.

For the ZnO/NF catalyst, the Joule heating increases the proportion of Zn^{2+} from 62.1% (under external heating) to 68.5%, and correspondingly decrease the proportion of Zn^0. The O 1s spectrum shows that Joule-heated catalyst exhibits a higher concentration of reactive oxygen species and Zn-O lattice oxygen, while the proportion of Ni-O lattice oxygen decreases. It indicates that Joule heating promotes the oxygen transferring from Ni-O lattice oxygen to the adsorbed oxygen and Zn-O lattice oxygen species, thus forms more adsorbed oxygen and ZnO. It is reported that the adsorbed oxygen would promote the adsorption of methanol on the ZnO stepped surface and reduce the potential barrier of O-H bond dissociation [56, 57]. Furthermore, the formation of ZnO on catalyst surface offers more active sites for methanol adsorption and dissociation, thus significantly enhances the catalytic reaction activity. This conclusion is supported by O_2-TPD experiments. As shown in Fig. S11, three types of desorption peaks can be observed. The peak below 150°C corresponds to physically adsorbed oxygen, the broad peak between 300-500°C belongs to chemically adsorbed oxygen, and the peak near 600°C is attributed to lattice oxygen [58-60]. Compared to external heating, the ZnO/NF catalyst treated with Joule heating exhibits a larger peak area for chemically adsorbed oxygen and a reduced peak area for lattice oxygen. This indicates that Joule heating promotes the release of lattice oxygen into adsorbed oxygen, which is consistent with the XPS results.

For the CuO/NF catalyst, its O 1s spectrum in Fig. 6c displays two distinct peaks at 531.1 eV and 529.4 eV, which are assigned to O_{ad} and O_{lat} (including Cu-O and Ni-O), respectively. Joule heating slightly increases the proportions of Cu^{2+} and O_{lat}, proving its ability to stimulate the release of bulk phase lattice oxygen to oxidize surface Cu species. Compared with ZnO/NF catalyst, Joule heating of CuO/NF has less effect on active metals and oxygen species. It has reported that the reductive Cu (Cu^+ and Cu^0 species) has higher catalytic activity than CuO with regards to the adsorption and activation of methanol molecules [53, 61]. Theoretically, Cu oxidization would decrease its activity. The kinetic analysis in Section 3.3 also reveals that the E_a of MD over CuO/NF is elevated under Joule heating. However, the methanol conversion under Joule heating is significantly higher. Under Joule heating, the current flows through the NF and supported metals. Since electrical resistance changes with the microstructure of catalyst, the Joule heating power differs across the catalyst positions. CuO/NF contains large amount of CuO nanoparticles, and the high contact resistance among particles generates “hot spots” at their contact surfaces when an electric current is applied [48-50]. These “hot spots” exhibit local temperature higher than the average temperature measured by a thermocouple. Different from the external heating, local temperature rise effect of the “hot spots” in Joule heating is an additional factor to promote methanol conversion.

In the case of CuO-ZnO/NF catalyst, compared with the samples in external heating, the proportions of Cu^{+}/Cu^{0} and Zn^{2+} on the catalyst surface increased after Joule heating as listed in Table S6. This shows that Joule heating promotes the reduction of Cu and the oxidation of Zn (Eq. (3)), and oxygen migration occurs between Cu and Zn, which would increase the number of active sites on the catalyst surface and enhance the methanol conversion. As mentioned above, no reduction of Cu is observed in the CuO/NF catalyst. It indicates that the addition of Zn promotes the reduction of Cu, and these two active metals have a synergistic effect in CuO-ZnO/NF catalyst. Meanwhile, Joule heating promotes the oxidation of Zn and thus prevents the formation of CuZn alloy, which inhibits the deactivation of catalyst. Studies have shown that the CuZn alloy exhibits low catalytic activity [51].

$$Cu^{2+} + Zn^{0} \rightarrow Cu^{+}/Cu^{0} + Zn^{2+}$$

Table 1

Surface atomic composition and ratio of CuO-ZnO/NF catalysts during electrification determined by in-situ XPS. (%)

sample	Cu 2p		Zn LMM		O 1s	
	Cu^{2+}	Cu^{+}/Cu^{0}	Zn^{2+}	Zn^{0}	O_{ad}	O_{lat}
0mA	24.8	75.2	65.4	34.6	28.1	71.9
10mA	18.0	82.0	66.7	33.3	23.7	76.3
0mA again	22.5	77.5	70.4	29.6	16.7	83.3

To further clarify the mechanisms, in-situ XPS analysis was conducted to analyze the change of CuO-ZnO/NF catalyst during electrification, and the results are shown in Fig. 6d-f and Table 1. It indicates that the Cu species are reduced and the Zn species are oxidized when applying a small current of 10 mA. These are consistent with the ex-situ XPS results of the catalyst treated by Joule heating for 1 h at a high current of about 17 A. When turning the power off, the valence states of Cu and Zn keep stable. The effect of electrified catalyst is an irreversible cumulative process. Notably, the Joule heating power in in-situ XPS (less than 0.2 mW) is too low to heat the catalyst. But

even a small current (10 mA) also alters the surface characteristic of active metals. These prove that except for Joule heating, the electrified catalyst when a current flows through a catalyst has an extra effect on the active sites, thus change its catalytic performance.

In-situ Raman was further performed to investigate the change of surface metal properties under different currents. Because the current in-situ cell cannot meet the requirements of Joule heating, a new cell equipped with two electrodes, gas inlet and outlet, etc. was self-manufactured, as shown in Fig. 7a and Fig. S12. The in-situ Raman spectrum of catalysts under Joule heating in an N_2 atmosphere is shown in Fig. 7b-d. On ZnO/NF catalyst, the intensities of Raman peaks at 96 cm^{-1} and 434 cm^{-1} in Fig.7b, corresponding to the crystal lattice vibrations of Zn-O, strengthen gradually with the increasing of electric current from 0 to 15 A. Besides, the proportions of peak area are calculated on the normalization method. As shown in Fig. 7e, the proportions of peaks at 96 cm^{-1} and 434 cm^{-1} increase, while those of peaks at 540 cm^{-1} and 1100 cm^{-1} corresponding to the defect structure and lattice vibration of NiO decrease with the increasing of current. Combined with XPS results, it reveals that Joule heating of ZnO/NF catalyst promotes the releasing of lattice oxygen in NiO and generates more ZnO. Raman peaks and their proportions on CuO/NF under various currents are shown in Fig. 7c and Fig. S13. There has little difference when applying different currents. The CuO/NF catalyst is stable during the Joule heating treatment. For CuO-ZnO/NF catalyst, when focusing on the rod-like structure, a weak peak at 203 cm^{-1}, corresponding to Cu_2O [62], increases with the effect of high current (the upper part of Fig. 7d and f). Besides, when examining a site on NF substrate, the peak at 294 cm^{-1}, corresponding to the CuO lattice vibration (A_{1g}), gradually decreases with the increasing of current as displayed in the lower part of Fig. 7d and f. It confirms that Joule heating can promote the reduction of Cu species on CuO-ZnO/NF catalyst. Compared with CuO/NF, the addition of Zn enhances the effect of Joule heating on Cu species.

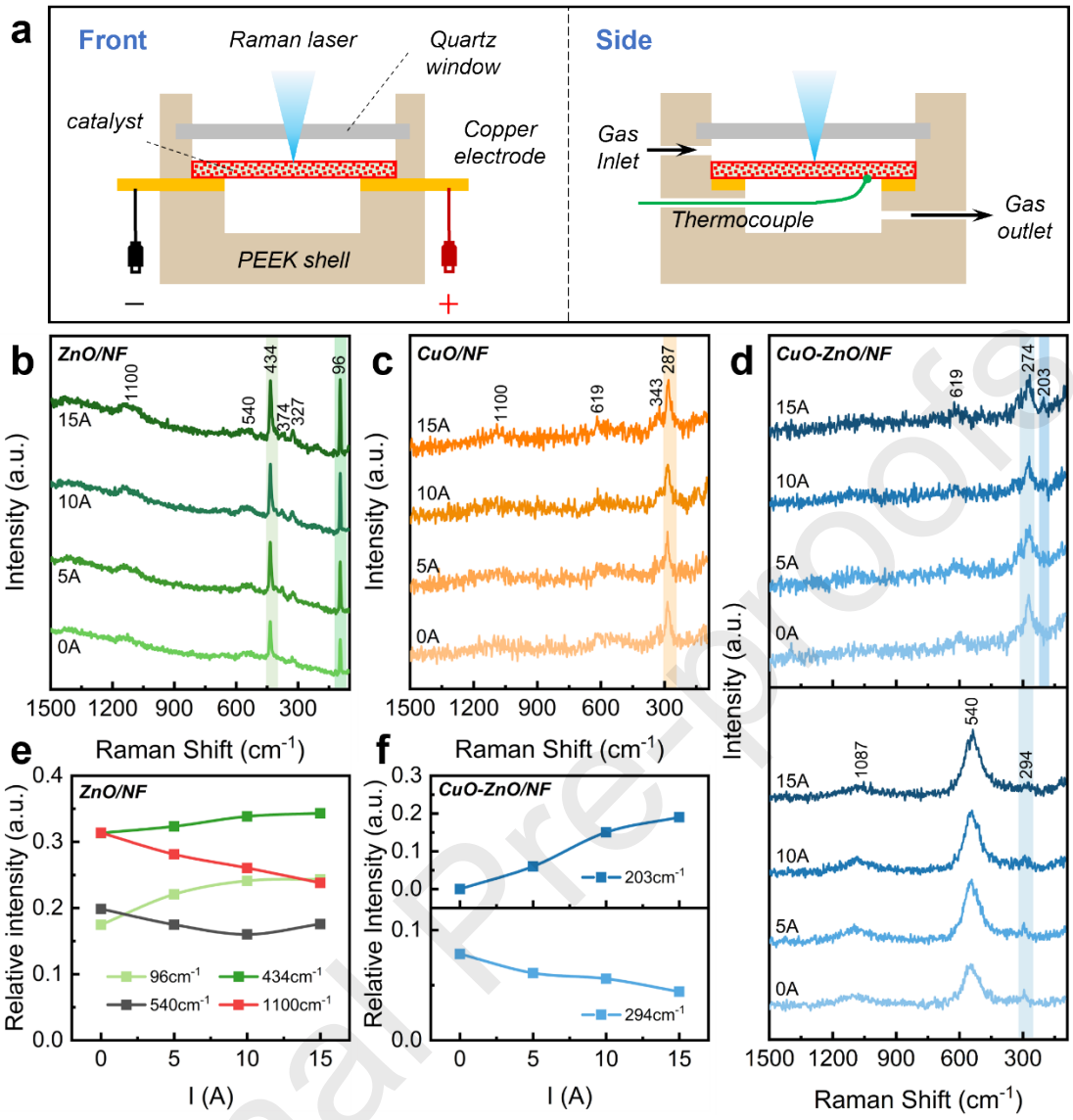

Fig. 7. (a) Diagram of a self-designed in-situ Raman reactor for Joule heating. In-situ Raman spectra under various currents of Joule heating: (b) ZnO/NF, (c) CuO/NF and (d) CuO-ZnO/NF. Normalized intensity of peaks during Joule heating: (e) ZnO/NF catalysts at 96 cm^{-1}, 434 cm^{-1}, 540 cm^{-1} and 1100 cm^{-1}; (f) CuO-ZnO/NF catalysts at 203 cm^{-1} and 294 cm^{-1}.

According to the above ex/in-situ characterizations, the promoting effects of Joule heating on methanol decomposition are summarized, as shown in Fig. 8. Firstly, the Joule heating can modify the catalyst structure as the electric current flows through the NF substrate and active metals. It has confirmed that the electrified ZnO/NF catalyst promotes the release of lattice oxygen (O_{lat}) from the NF matrix and generates more surface adsorbed oxygen (O_{ad}) and ZnO to improve methanol conversion. With regards to the bimetallic CuO-ZnO/NF catalyst, Joule heating facilitates redox reactions

between Cu and Zn species, which forms more active sites of ZnO and Cu^{+}/Cu^{0} for MD. Secondly, Joule heating generates "hotspots" at high-resistance particle contact surfaces, as shown by the red area among particles in Fig. 8. For the CuO/NF catalyst, Joule heating promotes Cu oxidation and increases activation energy. However, the local temperature rise at hotspots enhances methanol conversion. The localized high-temperature effect of hotspots in Joule heating is another key factor enhancing methanol conversion for all three catalysts.

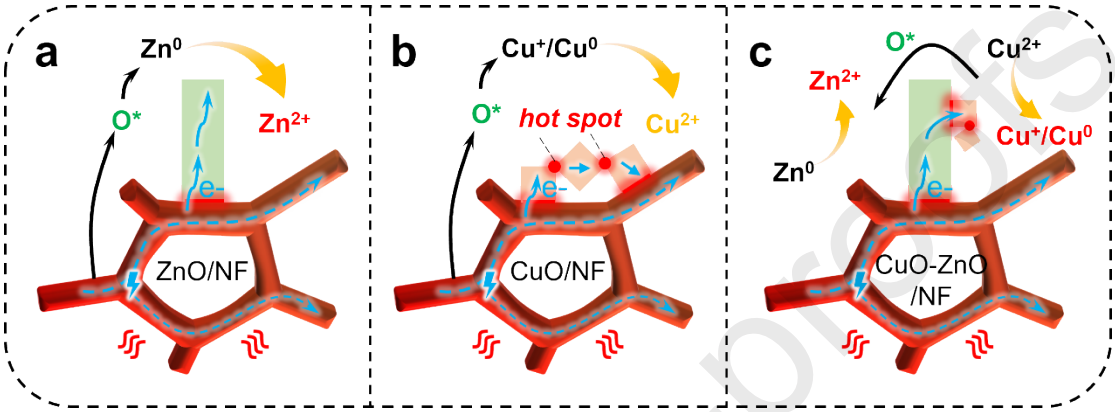

Fig. 8. Promoting mechanism of Joule heating (a) ZnO/NF, (b) CuO/NF and (c) CuO-ZnO/NF catalysts.

4 Conclusion

The new method of Joule heating promoted methanol decomposition over metal skeleton catalysts offers a flexible, efficient, and energy-saving approach for H_2 production. The heating property, catalytic performance, and the promoting mechanism of Joule heating over CuO-ZnO/NF, ZnO/NF, and CuO/NF were investigated. The maximum heating and cooling rates achieved through Joule heating are 12°C/s and 17°C/s, respectively. Its start-stop cycle time is just 1/8 of that required for conventional external heating. Besides, methanol conversion of CuO-ZnO/NF under Joule heating at 300°C remarkably increases by 88% in comparison with that under external heating, while the energy consumption of Joule heating is only 29% of that of external heating. The less energy consumption of Joule heating is attributed to the low surface temperature of the reactor, which decreases the energy loss of external free convection and radiative heat transfer. The higher catalytic activity is due to the extra effects of Joule heating which promotes the migration of oxygen and redox of Cu/Zn species, and generates the "hot spot" effect to rise the local temperature.

Author contributions

All authors contributed to the study conception and design. Material preparation, data collection, and analysis were performed by Xuechen Zhou. Investigation and formal analysis were performed by Chiyu Wang and Yufan Yang. Conceptualization, methodology, validation and funding acquisition were performed by Limo He.

Supervision and project administration were performed by Song Hu. Writing – review & editing were performed by Yanglin Chen, Sam Fong Yau Li, Yifei Sun, Sheng Su and Yi Wang. Writing – review & editing and project administration were performed by Jun Xiang. The first draft of the manuscript was written by Xuechen Zhou and all authors commented on previous versions of the manuscript. All authors read and approved the final manuscript.

Conflicts of interest

The authors declare no competing financial interest.

Acknowledgements

This research was supported by the National Natural Science Foundation of China (No. 52376189). The assistance from the Analysis and Testing Center of Huazhong University of Science and Technology and the State Key Laboratory of Physical Chemistry of Solid Surface of Xiamen University was also highly recognized.

References

[1] D. Shindell, C.J. Smith, Climate and air-quality benefits of a realistic phase-out of fossil fuels, Nature 573(7774) (2019) 408-411. https://doi.org/10.1038/s41586-019-1554-z.

[2] K. Sun, Y. Qian, H.L. Jiang, Metal-organic frameworks for photocatalytic water splitting and CO_2 reduction, Angew. Chem. 135(15) (2023) e202217565. https://doi.org/10.1002/anie.202217565.

[3] Z. Abdin, A. Zafaranloo, A. Rafiee, W. Mérida, W. Lipiński, K.R. Khalilpour, Hydrogen as an energy vector, Renewable Sustainable Energy Rev. 120 (2020) 109620. https://doi.org/10.1016/j.rser.2019.109620.

[4] F. Cai, Y. Guo, J.J. Ibrahim, J. Zhang, Y. Sun, A highly active and stable Pd/MoC catalyst for hydrogen production from methanol decomposition, Appl. Catal., B 299 (2021) 120648. https://doi.org/10.1016/j.apcatb.2021.120648.

[5] L. Lin, W. Zhou, R. Gao, S. Yao, X. Zhang, W. Xu, S. Zheng, Z. Jiang, Q. Yu, Y.-W. Li, C. Shi, X.-D. Wen, D. Ma, Low-temperature hydrogen production from water and methanol using Pt/α-MoC catalysts, Nature 544(7648) (2017) 80-83. https://doi.org/10.1038/nature21672.

[6] Z. Sun, S. Yu, S. Toan, R. Abiev, M. Fan, Z. Sun, Enabling low-temperature methanol activation via lattice oxygen induced Cu-O-Cr catalysis, ACS Catal. 13(20) (2023) 13704-13716. https://doi.org/10.1021/acscatal.3c03054.

[7] H.F. Abbas, W.M.A. Wan Daud, Hydrogen production by methane decomposition:

A review, Int. J. Hydrogen Energy 35(3) (2010) 1160-1190. https://doi.org/10.1016/j.ijhydene.2009.11.036.

[8] D. Kang, J.W. Lee, Enhanced methane decomposition over nickel-carbon-B_2O_3 core-shell catalysts derived from carbon dioxide, Appl. Catal., B 186 (2016) 41-55. https://doi.org/10.1016/j.apcatb.2015.12.045.

[9] N. Li, C. Zhang, D. Li, W. Jiang, F. Zhou, Review of reactor systems for hydrogen production via ammonia decomposition, Chem. Eng. J. 495 (2024) 153125. https://doi.org/10.1016/j.cej.2024.153125.

[10] N. Köwitsch, L. Thoni, B. Klemmed, A. Benad, P. Paciok, M. Heggen, I. Köwitsch, M. Mehring, A. Eychmüller, M. Armbrüster, Proving a paradigm in methanol steam reforming: catalytically highly selective InxPdy/In_2O_3 interfaces, ACS Catal. 11(1) (2021) 304-312. https://doi.org/10.1021/acscatal.0c04073.

[11] X. Li, D. Yuan, T. Xie, Q. Zhang, W. Xu, T. Fu, X. Chu, T. Luo, L. Wu, W. Zhou, UV-Laser ablation enhanced Joule-heating catalyst support for electrified MSR in microreactor, Chem. Eng. J. 459 (2023) 141571. https://doi.org/10.1016/j.cej.2023.141571.

[12] S. Sollai, A. Porcu, V. Tola, F. Ferrara, A. Pettinau, Renewable methanol production from green hydrogen and captured CO_2: A techno-economic assessment, J. CO_2 Util. 68 (2023) 102345. https://doi.org/10.1016/j.jcou.2022.102345.

[13] T. Li, Y. Meng, L. Yin, B. Sun, W. Zhu, J. Su, K. Wang, Synthesis of sustainable aviation biofuels via catalytic hydropyrolysis of lignin, Appl. Catal., B 353 (2024) 124092. https://doi.org/10.1016/j.apcatb.2024.124092.

[14] Y. Chen, M. Zheng, J. Sun, J. Xu, C. Wu, J. Liu, L. He, S. Xi, S. Li, C. Xue, Photoreforming of lignocellulose into CO and lactic acid over a single-atom Fe-dispersed order/disorder polymeric carbon nitride homojunction, ACS Catal. 14 (2024) 17321-17330. https://doi.org/10.1021/acscatal.4c05510.

[15] M. Turco, G. Bagnasco, C. Cammarano, P. Senese, U. Costantino, M. Sisani, Cu/ZnO/Al_2O_3 catalysts for oxidative steam reforming of methanol: The role of Cu and the dispersing oxide matrix, Appl. Catal., B 77(1) (2007) 46-57. https://doi.org/10.1016/j.apcatb.2007.07.006.

[16] G. Garcia, E. Arriola, W.-H. Chen, M.D. De Luna, A comprehensive review of hydrogen production from methanol thermochemical conversion for sustainability, Energy 217 (2021) 119384. https://doi.org/10.1016/j.energy.2020.119384.

[17] S. Sá, H. Silva, L. Brandão, J.M. Sousa, A. Mendes, Catalysts for methanol steam

reforming-A review, Appl. Catal., B 99(1) (2010) 43-57. https://doi.org/10.1016/j.apcatb.2010.06.015.

[18] S. Luo, H. Song, F. Ichihara, M. Oshikiri, W. Lu, D.-M. Tang, S. Li, Y. Li, Y. Li, P. Davin, T. Kako, H. Lin, J. Ye, Light-Induced dynamic restructuring of Cu active sites on TiO_2 for low-temperature H_2 production from methanol and water, J. Am. Chem. Soc. 145(37) (2023) 20530-20538. https://doi.org/10.1021/jacs.3c06688.

[19] Y.T. Kim, J.-J. Lee, J. Lee, Electricity-driven reactors that promote thermochemical catalytic reactions via joule and induction heating, Chem. Eng. J. 470 (2023) 144333. https://doi.org/10.1016/j.cej.2023.144333.

[20] S.T. Wismann, J.S. Engbæk, S.B. Vendelbo, F.B. Bendixen, W.L. Eriksen, K. Aasberg-Petersen, C. Frandsen, I. Chorkendorff, P.M. Mortensen, Electrified methane reforming: A compact approach to greener industrial hydrogen production, Science 364(6442) (2019) 756-759. https://doi.org/10.1126/science.aaw8775.

[21] D. Mei, X. Qiu, H. Liu, Q. Wu, S. Yu, L. Xu, T. Zuo, Y. Wang, Progress on methanol reforming technologies for highly efficient hydrogen production and applications, Int. J. Hydrogen Energy 47(84) (2022) 35757-35777. https://doi.org/10.1016/j.ijhydene.2022.08.134.

[22] Z. Zhang, Y. Le, L. Jing, G. Huang, J. Kang, Q. Zhang, Y. Wang, Foam-structured Fe catalysts for enhanced heat and mass transfer in synthesis of olefins from syngas, Appl. Catal., B 361 (2025) 124569. https://doi.org/10.1016/j.apcatb.2024.124569.

[23] X. Tang, C. Song, H. Li, W. Liu, X. Hu, Q. Chen, H. Lu, S. Yao, X.-n. Li, L. Lin, Thermally stable Ni foam-supported inverse $CeAlO_x$/Ni ensemble as an active structured catalyst for CO_2 hydrogenation to methane, Nat. Commun. 15(1) (2024) 3115. https://doi.org/10.1038/s41467-024-47403-4.

[24] M. Ambrosetti, A. Beretta, G. Groppi, E. Tronconi, A numerical investigation of electrically-heated methane steam reforming over structured catalysts, Front. Chem. Eng. 3 (2021) 747636. https://doi.org/10.3389/fceng.2021.747636.

[25] Q. Ma, Y. Gao, B. Sun, J. Du, H. Zhang, D. Ma, Grave-to-cradle dry reforming of plastics via Joule heating, Nat. Commun. 15(1) (2024) 8243. https://doi.org/10.1038/s41467-024-52515-y.

[26] C. Tao, L. He, X. Zhou, Y. Yang, H. Li, Q. Ren, S. Hu, K. Xu, L. Jiang, J. Xu, S. Su, Y. Wang, J. Xiang, Experimental and mechanistic studies on the thermo-electric synergistic catalytic oxidation of acetone over MnO_2/TiO_2-Ni foam catalyst, Chem. Eng. J. 488 (2024) 150805.

https://doi.org/10.1016/j.cej.2024.150805.

[27] L. Zheng, M. Ambrosetti, E. Tronconi, Joule-heated catalytic reactors toward decarbonization and process intensification: A Review, ACS Eng. Au 4(1) (2024) 4-21. https://doi.org/10.1021/acsengineeringau.3c00045.

[28] R. Daiyan, I. MacGill, R. Amal, Opportunities and Challenges for Renewable Power-to-X, ACS Energy Lett. 5(12) (2020) 3843-3847. https://doi.org/10.1021/acsenergylett.0c02249.

[29] L. Zheng, M. Ambrosetti, F. Zaio, A. Beretta, G. Groppi, E. Tronconi, Direct electrification of Rh/Al_2O_3 washcoated SiSiC foams for methane steam reforming: An experimental and modelling study, Int. J. Hydrogen Energy 48(39) (2023) 14681-14696. https://doi.org/10.1016/j.ijhydene.2022.12.346.

[30] Y.R. Lu, P.A. Nikrityuk, Steam methane reforming driven by the Joule heating, Chem. Eng. Sci. 251 (2022) 117446. https://doi.org/10.1016/j.ces.2022.117446.

[31] E.B. Ledesma, M. Idamakanti, P. Bollini, M.P. Harold, R.R.J.C. Ratnakar, Decarbonizing steam-methane reforming: Enhancing activity through Joule heating of a Ni/ZrO_2-coated FeCrAl coil, ChemCatChem 16(8) (2024) e202301110. https://doi.org/10.1002/cctc.202301110.

[32] N. Zou, Q. Nie, X. Zhang, G. Zhang, J. Wang, P. Zhang, Electrothermal regeneration by Joule heat effect on carbon cloth based MnO_2 catalyst for long-term formaldehyde removal, Chem. Eng. J. 357 (2019) 1-10. https://doi.org/10.1016/j.cej.2018.09.117.

[33] K. Wang, Y. Zeng, W. Lin, X. Yang, Y. Cao, H. Wang, F. Peng, H. Yu, Energy-efficient catalytic removal of formaldehyde enabled by precisely Joule-heated Ag/Co_3O_4@mesoporous-carbon monoliths, Carbon 167 (2020) 709-717. https://doi.org/10.1016/j.carbon.2020.06.055.

[34] X. Mei, X. Zhu, Y. Zhang, Z. Zhang, Z. Zhong, Y. Xin, J. Zhang, Decreasing the catalytic ignition temperature of diesel soot using electrified conductive oxide catalysts, Nat. Catal. 4(12) (2021) 1002-1011. https://doi.org/10.1038/s41929-021-00702-1.

[35] A. Badakhsh, Y. Kwak, Y.-J. Lee, H. Jeong, Y. Kim, H. Sohn, S.W. Nam, C.W. Yoon, C.W. Park, Y.S. Jo, A compact catalytic foam reactor for decomposition of ammonia by the Joule-heating mechanism, Chem. Eng. J. 426 (2021) 130802. https://doi.org/10.1016/j.cej.2021.130802.

[36] L. Dou, C. Yan, L. Zhong, D. Zhang, J. Zhang, X. Li, L. Xiao, Enhancing CO2 methanation over a metal foam tructured catalyst by electric internal heating,

Chem. Commun. 56(2) (2019) 205-208. https://doi.org/10.1039/c9cc07525a.

[37] P. Du, R. Wang, B. Deng, X. He, Y. Long, C. Yang, Z. Wang, B. Ge, K. Huang, R. Zhang, M. Lei, H. Wu, In-situ Joule-heating drives rapid and on-demand catalytic VOCs removal with ultralow energy consumption, Nano Energy 102 (2022) 107725. https://doi.org/10.1016/j.nanoen.2022.107725.

[38] L. He, X. Yin, C. Tao, X. Zhou, Q. Ren, J. Xu, S. Hu, S. Su, Y. Wang, J. Xiang, Self-assembly of CNTs@Ni foam electrode material and its activation effect during catalytic reforming of bio-oil model compound for hydrogen at different temperatures, Fuel 336 (2023) 127155. https://doi.org/10.1016/j.fuel.2022.127155.

[39] J. Zhang, S. Hu, Y. Ding, R. Huang, Q. Ren, S. Su, Y. Wang, L. Jiang, J. Xu, J. Xiang, Nickel based catalyst supported by carbon aerogel prepared from waste pomelo peel to crack ethanol for hydrogen production: Catalytic performance and mechanism, Fuel 346 (2023) 128278. https://doi.org/10.1016/j.fuel.2023.128278.

[40] L.J. Oblonsky, T.M. Devine, Surface Enhanced Raman Spectra from the Films Formed on Nickel in the Passive and Transpassive Regions, J. Electrochem. Soc. 142(11) (1995) 3677. https://doi.org/10.1149/1.2048398.

[41] S. Lee, Y.-C. Chu, L. Bai, H.M. Chen, X. Hu, Operando identification of a side-on nickel superoxide intermediate and the mechanism of oxygen evolution on nickel oxyhydroxide, Chem Catal. 3(1) (2023) 100475. https://doi.org/10.1016/j.checat.2022.11.014.

[42] C. Li, T. Ahmed, M. Ma, T. Edvinsson, J. Zhu, A facile approach to ZnO/CdS nanoarrays and their photocatalytic and photoelectrochemical properties, Appl. Catal., B 138 (2013) 175-183. https://doi.org/10.1016/j.apcatb.2013.02.042.

[43] Y. Deng, A.D. Handoko, Y. Du, S. Xi, B.S. Yeo, In situ Raman spectroscopy of copper and copper oxide surfaces during electrochemical oxygen evolution reaction: Identification of CuIII oxides as catalytically active species, ACS Catal. 6(4) (2016) 2473-2481. https://doi.org/10.1021/acscatal.6b00205.

[44] J.X. Wang, X.W. Sun, Y. Yang, K.K.A. Kyaw, X.Y. Huang, J.Z. Yin, J. Wei, H.V. Demir, Free-standing ZnO-CuO composite nanowire array films and their gas sensing properties, Nanotechnology 22(32) (2011) 325704. https://doi.org/10.1088/0957-4484/22/32/325704.

[45] J. Xu, W. Ji, Z. Shen, W.S. Li, S.H. Tang, X. Ye, D.Z. Jia, X. Xin, Raman spectra of CuO nanocrystals, J. Raman Spectrosc. 30 (1999) 413-415. https://doi.org/10.1002/(SICI)1097-4555(199905)30:5<413::AID-JRS387>3.0.CO;2-N.

[46] S. Kuld, M. Thorhauge, H. Falsig, C.F. Elkjær, S. Helveg, I. Chorkendorff, J. Sehested, Quantifying the promotion of Cu catalysts by ZnO for methanol synthesis, Science 352(6288) (2016) 969-974. https://doi.org/10.1126/science.aaf0718.

[47] J. Wang, H. Liu, T. Wang, Y. Xi, P. Sun, F. Li, Boosting CO_2 hydrogenation to methanol via Cu-Zn synergy over highly dispersed Cu, Zn-codoped ZrO_2 catalysts, Catal. Today 410 (2023) 205-214. https://doi.org/10.1016/j.cattod.2022.05.034.

[48] K. Maize, S.R. Das, S. Sadeque, A. Mohammed, A. Shakouri, D.B. Janes, M.A. Alam, Super-Joule heating in graphene and silver nanowire network, Appl. Phys. Lett. 106(14) (2015) 143104. https://doi.org/10.1063/1.4916943.

[49] B. Deng, P.A. Advincula, D.X. Luong, J. Zhou, B. Zhang, Z. Wang, E.A. McHugh, J. Chen, R.A. Carter, C. Kittrell, J. Lou, Y. Zhao, B.I. Yakobson, Y. Zhao, J.M. Tour, High-surface-area corundum nanoparticles by resistive hotspot-induced phase transformation, Nat. Commun. 13(1) (2022) 5027. https://doi.org/10.1038/s41467-022-32622-4.

[50] Q. Xiong, X. Zhu, R. He, X. Mei, Y. Zhang, Z. Zhong, W. Zhao, W. Nie, J. Zhang, Local Joule heating targets catalyst surface for hydrocarbon combustion, J. Ind. Eng. Chem. 117 (2023) 273-281. https://doi.org/10.1016/j.jiec.2022.10.016.

[51] D. Li, F. Xu, X. Tang, S. Dai, T. Pu, X. Liu, P. Tian, F. Xuan, Z. Xu, I.E. Wachs, M. Zhu, Induced activation of the commercial $Cu/ZnO/Al_2O_3$ catalyst for the steam reforming of methanol, Nat. Catal. 5(2) (2022) 99-108. https://doi.org/10.1038/s41929-021-00729-4.

[52] G. Hu, J. Wang, D. Liu, X. Zhang, B. Yu, T. Huang, M. Zhu, H. Yu, A Joule-heated carbon nanofiber aerogel-supported catalyst for hydrogen production via methanol steam reforming, Carbon 214 (2023) 118311. https://doi.org/10.1016/j.carbon.2023.118311.

[53] S.D. Jones, L.M. Neal, H.E. Hagelin-Weaver, Steam reforming of methanol using Cu-ZnO catalysts supported on nanoparticle alumina, Appl. Catal., B 84(3) (2008) 631-642. https://doi.org/10.1016/j.apcatb.2008.05.023.

[54] T.J. Frankcombe, Y. Liu, Interpretation of oxygen 1s X-ray photoelectron spectroscopy of ZnO, Chem. Mater. 35(14) (2023) 5468-5474. https://doi.org/10.1021/acs.chemmater.3c00801.

[55] B.P. Payne, M.C. Biesinger, N.S. McIntyre, Use of oxygen/nickel ratios in the XPS characterisation of oxide phases on nickel metal and nickel alloy surfaces, J. Electron Spectrosc. Relat. Phenom. 185(5) (2012) 159-166. https://doi.org/10.1016/j.elspec.2012.06.008.

[56] S. Mehta, K. Joshi, Electronic fingerprints for diverse interactions of methanol with various Zn-based systems, Surf. Sci. 736 (2023) 122350. https://doi.org/10.1016/j.susc.2023.122350.

[57] S. Mehta, K. Joshi, From molecular adsorption to decomposition of methanol on various ZnO facets: A periodic DFT study, Appl. Surf. Sci. 602 (2022) 154150. https://doi.org/10.1016/j.apsusc.2022.154150.

[58] M. Adeel, M. Saeed, I. Khan, M. Muneer, N. Akram, Synthesis and characterization of Co–ZnO and evaluation of its photocatalytic activity for photodegradation of methyl orange, ACS Omega 6(2) (2021) 1426-1435. https://doi.org/10.1021/acsomega.0c05092.

[59] S. Song, H. Song, L. Li, S. Wang, W. Chu, K. Peng, X. Meng, Q. Wang, B. Deng, Q. Liu, Z. Wang, Y. Weng, H. Hu, H. Lin, T. Kako, J. Ye, A selective Au-ZnO/TiO_2 hybrid photocatalyst for oxidative coupling of methane to ethane with dioxygen, Nat. Catal. 4(12) (2021) 1032-1042. https://doi.org/10.1038/s41929-021-00708-9.

[60] H. Wang, H. Zhang, J. Zhang, J.P. Han, H. Fang, M.H. Yu, Z. Chang, X.H. Bu, Innovative microstructure and morphology engineering of MOF-derived single-atom Sn-doped ZnO nanosheet showing highly sensitive acetone sensing, Adv. Funct. Mater. (2025) 2422378. https://doi.org/10.1002/adfm.202422378.

[61] F. Chen, P. Zhang, Y. Zeng, R. Kosol, L. Xiao, X. Feng, J. Li, G. Liu, J. Wu, G. Yang, Y. Yoneyama, N. Tsubaki, Vapor-phase low-temperature methanol synthesis from CO_2-containing syngas via self-catalysis of methanol and Cu/ZnO catalysts prepared by solid-state method, Appl. Catal., B 279 (2020) 119382. https://doi.org/10.1016/j.apcatb.2020.119382.

[62] S. Shyamal, A. Maity, A.K. Satpati, C. Bhattacharya, Amplification of PEC hydrogen production through synergistic modification of Cu_2O using cadmium as buffer layer and dopant, Appl. Catal., B 246 (2019) 111-119. https://doi.org/10.1016/j.apcatb.2019.01.017.

Declaration of interests

☒ The authors declare that they have no known competing financial interests or personal relationships that could have appeared to influence the work reported in this paper.

☐ The authors declare the following financial interests/personal relationships which may be considered as potential competing interests:

Graphical Abstract

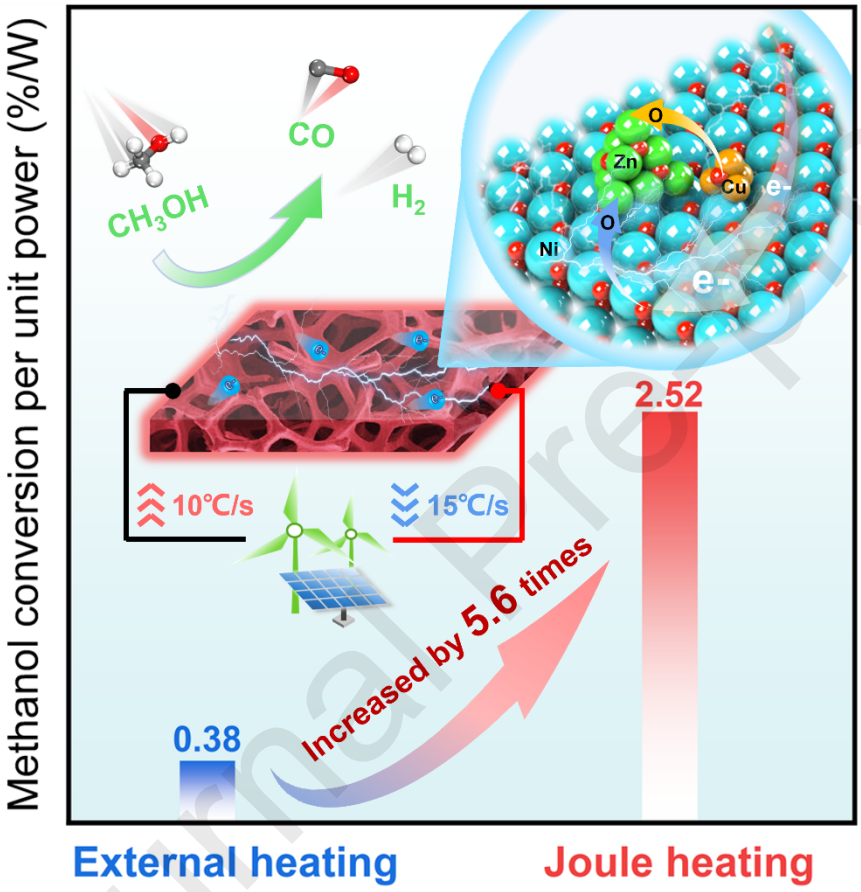

Highlights

- Joule heating rates of metal skeleton catalysts above 10°C/s
- Joule heating method improves methanol conversion by over 80% at 300°C
- Energy consumption of Joule heating at 300°C is 29% of that by external heating
- Joule heating promotes the migration of oxygen and redox of Cu/Zn species

827